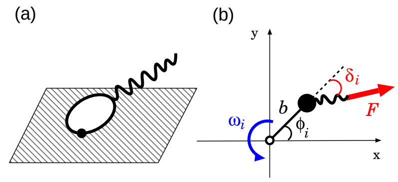

FIG. 1: Schematic picture of the rotor (top view). The active force $\boldsymbol{F}_i$ exerted by the i-th rotor on the fluid is deviated by a fixed angle δ_i from the radial direction. The reaction force drives the rotor at the intrinsic frequency $\omega_i = F\sin\delta_i/\zeta b$, where b is the radius of rotation and ζ the viscous drag coefficient of the bead.

tally (flagellum). Motion of the bead is constrained on a circular orbit of radius b located at height h from the substrate, which we take to be the xy-plane. The position of the i-th bead is thus given by $\mathbf{r}_i = \mathbf{r}_{0i} + h\boldsymbol{e}_z + b\boldsymbol{n}_i$ where $\mathbf{r}_{0i}$ is its base position on the square lattice and $\boldsymbol{n}_i = (\cos\phi_i, \sin\phi_i, 0)$ is the unit vector that gives the orientation of the arm via its phase $\phi_i = \phi_i(t)$. The velocity of the bead reads $\mathbf{v}_i = \dot{\phi}_i \boldsymbol{t}_i$ where $\boldsymbol{t}_i = (-\sin\phi_i, \cos\phi_i, 0)$ is the unit vector tangential to the trajectory. We assume that the active force $\boldsymbol{F}_i$ exerted by the rotor on the fluid has a constant magnitude F, and makes a fixed angle δ_i (measured clockwise) from the radial direction; $\boldsymbol{F}_i = F(\cos\delta_i \boldsymbol{n}_i - \sin\delta_i \boldsymbol{t}_i)$. See Fig. 1 for the configuration. The reaction force $-\boldsymbol{F}_i$ on the rotor arm gives the driving torque $T_i = Fb\sin\delta_i$ and the intrinsic frequency $\omega_i = F\sin\delta_i/\zeta b$, where $\zeta = 6\pi\eta a$ is the viscous drag coefficient. The mounting angles δ_i's are assumed to have the Gaussian distribution

$$P(\delta) = \frac{1}{\sqrt{2\pi}\delta_0}\exp\left(-\frac{\delta^2}{2\delta_0^2}\right) \quad (1)$$

with the standard deviation δ_0.

We assume that the rotors are widely spaced so that $a, b, h \ll d$. Then the velocity field of the fluid created by the active forces is given by $\mathbf{v}(\mathbf{r}) = \sum_i \mathbf{G}(\mathbf{r} - \mathbf{r}_i)\cdot\boldsymbol{F}_i$, where $\mathbf{G}(\mathbf{r}) = (3h^2/2\pi\eta)\cdot \mathbf{r}_\perp\mathbf{r}_\perp/|\mathbf{r}|^5$, $\mathbf{r}_\perp = (x, y, 0)$ is the asymptotic expression of the Oseen-Blake tensor [23] for $h/d \ll 1$. The rotor's angular velocity is given by $\omega_i + \mathbf{v}(\mathbf{r}_i)\cdot \boldsymbol{t}_i/b$, or, more explicitly,

$$\begin{aligned} \frac{d\phi_i}{dt} &= \omega_0 \sin\delta_i - \frac{3\gamma\omega_0 d^3}{4\pi}\sum_{j\neq i}\frac{1}{|\mathbf{r}_{ij}|^3}\Big[\sin(\phi_i - \phi_j + \delta_j) \\ &\quad + \cos(\phi_i + \phi_j - \delta_j - 2\theta_{ij})\Big]. \end{aligned} \quad (2)$$

Here, $\omega_0 = F/\zeta b$, $\mathbf{r}_{ij} = \mathbf{r}_i - \mathbf{r}_j = |\mathbf{r}_{ij}|(\cos\theta_{ij}, \sin\theta_{ij})$, and $\gamma = \zeta h^2/\eta d^3 = 6\pi a h^2/d^3$ is the dimensionless coupling constant. For a real bacterial carpet, $a \sim h \sim 1\mu$m and $d \sim 10\mu$m give the rough estimate $\gamma \sim 10^{-2}$.

Numerical Simulation. - We implemented the model on a $L \times L$ square lattice and numerically integrated eq. (2) by the Euler method. We assumed the periodic boundary condition and computed the velocity field every time step in the Fourier space. We set $\gamma = 0.1$ and varied the angle deviation δ_0 as the control parameter. The system size used was $L = 128$ for most of the results shown below, while $L = 32$, 64 and 256 are also used to check finite-size effect. Starting from random initial configurations of $\phi_i(t = 0)$, the system reached a dynamical steady state by the time $t = 1\times 10^4/\omega_0$. The statistical data shown below are taken from the time window $1\times 10^4 < \omega_0 t < 2.5\times 10^5$.

We plot the orientational order parameter $S = |\langle \boldsymbol{n}\rangle| = |\langle e^{i\phi}\rangle|$ as a function of δ_0 in Fig. 2. Also shown is the standard deviation (STD) of the actual frequency $\Omega_i = \langle\dot{\phi}_i\rangle$ normalized by the STD of the intrinsic frequency ω_i, $Q = \sqrt{\langle\Omega^2\rangle/\langle\omega^2\rangle}$. Note that $S = 1$ and $Q = 0$ in the fully synchronized state and $S = 0$ and $Q = 1$ in the desynchronized limit. As we increase δ_0, S and Q slowly converge to the desynchronized limit. While the change in the orientational order parameter is sharper for a larger system size, the frequency deviation has little L-dependence. For comparison, we also show the results of the mean-field theory, which will be explained in the next section.

In Fig. 3, we plot the distribution function of the actual frequency Ω normalized by the STD of intrinsic frequency, for different values of δ_0. The distribution consists of a sharp delta-function like peak at $\Omega = 0$ and broad symmetric tails for $\Omega > 0$ and $\Omega < 0$. For $\delta_0 \leq 3°$, most of the rotors are coherent and contribute to the center-peak. For $\delta_0 = 10°$, the distribution is close to that of the intrinsic frequency, while the center peak still remains. the above data suggest that the synchronization transition in this system is more gradual than that found in a globally coupled system, and it is difficult to locate the transition point exactly.

On the other hand, the variance of the order parameter $\mathrm{Var}(S) = \langle S(t)^2\rangle - \langle S(t)\rangle^2$ as a function of δ_0 (Fig. 4(a)) has a peak near $\delta_0 = 6°$, suggesting that there is a subtle balance between synchronization and desynchronization. We will call this the threshold angle and denote by δ_{th}.

In Fig.4(b), we plot the temporal correlation function of the order parameter $C_S(t) = \langle S(t+t')S(t')\rangle - \langle S\rangle^2$. We find an oscillatory behavior with long correlation time at $\delta_0 = 6°$. The presence of a characteristic period is also directly observed in the plot of $S(t)$ in Fig. 4(c). Although the origin of the oscillation is beyond the scope of the present paper, a preliminary study shows that the oscillatory behavior at the threshold angle is a unique feature resulting from the long-ranged nature of the interaction.

We also plot the orientational correlation function

$$G_n(|\mathbf{r}|) = \langle[\boldsymbol{n}(\mathbf{r}+\mathbf{r}') - \overline{\boldsymbol{n}}]\cdot[\boldsymbol{n}(\mathbf{r}') - \overline{\boldsymbol{n}}]\rangle \quad (3)$$

in Fig.5. Here the angular brackets mean taking average over $\mathbf{r}'$ as well as the azimuthal angle of $\mathbf{r}$. For $4 \leq \delta_0 \leq 6°$, we observe an exponential decay of the correlation